Resonance energy transfer dynamics in hydrogen-bonded oligo-*p*-phenylenevinylene nanostructures

Clément Daniel[a], Laura M. Herz[b], David Beljonne[c], Freek J.M. Hoeben[d], Pascal Jonkheijm[d], Albertus P.H.J. Schenning[d], E.W. Meijer[d], Richard T. Phillips[a], Carlos Silva[a,*]

[a] *Cavendish Laboratory, University of Cambridge, Madingley Road, Cambridge CH3 0HE, UK*
[b] *Clarendon Laboratory, University of Oxford, Parks Road, Oxford OX1 3PU, UK*
[c] *Chemistry of Novel Materials, University of Mons-Hainaut, Place du Parc 20, B-7000 Mons, Belgium*
[d] *Laboratory of Macromolecular and Organic Chemistry, Eindhoven University of Technology, P.O. Box 513, 5600 MB Eindhoven, The Netherlands*

Abstract

Oligo-*p*-phenylenevinylene (OPV) materials monofunctionalised with ureido-*s*-triazine form chiral, helical stacks in dodecane solution. Here, we investigate resonance energy transfer dynamics in supramolecular stacks of OPVs consisting of three phenyl rings (MOPV3) doped with similar oligomers containing four phenyl rings (MOPV4). Broad spectral overlap between the MOPV3 fluorophores and MOPV4 chromophores results in efficient energy transfer from MOPV3 to MOPV4. We observe resonance energy transfer following two distinct regimes. The first is evident by growth of MOPV4 photoluminescence on a timescale of ∼50 ps, mediated by rapid exciton diffusion in MOPV3 within the stack. In the second regime, dynamics of localised excitons on nanosecond timescales are dominated by direct resonance energy transfer to MOPV4 chromophores. Global analysis of the photoluminescence decay of MOPV3 in blends with varying MOPV4 composition on times $\gtrsim 2$ ns is consistent with quasi-one-dimensional resonance energy transfer with Förster radius of 8 nm.

1. Introduction

Polymeric semiconductor materials are now widely used in optoelectronic devices such as field-effect transistors [1], light-emitting diodes [2], and photovoltaic diodes [3]. Intramolecular functionality (π-conjugation) can be tailored with synthetic methodologies [4–6], but control of intermolecular properties, which are equally important in determining electronic properties (e.g. charge transport [7]), is more elusive. Perhaps the most compelling advantage of many organic semiconductors such as conjugated polymers

over molecular and inorganic semiconductors is solution processability, making fabrication of elegantly simple device structures possible with techniques such as ink-jet printing [8,9]. A natural strategy to achieve three-dimensional control of intermolecular interactions is to exploit molecular self assembly in solution prior to the casting process by means of supramolecular chemistry [10]. With this approach, molecular building blocks are self-assembled to form well-defined, complex architectures through secondary forces, such as hydrophilic or hydrophobic interactions, hydrogen bonding, and Coulombic interactions. These interactions need to be strong enough to lead to spontaneous self-organisation but weak enough so that the process is reversible. Supramolecular assemblies may be designed to

---

* Corresponding author.
E-mail address: cs271@cam.ac.uk (C. Silva).

possess polymeric characteristics and are therefore often referred to as "supramolecular polymers". Their macroscopic properties can be tuned such that high carrier mobilities, for example, can be achieved [11].

Recently, this approach has been applied very successfully to oligo(p-phenylene-vinylene) derivatives with chiral side-chains and functionalised with ureido-s-triazine, a hydrogen-bonding end-group [12]. It has been shown that these monofunctionalized oligo(p-phenylenevinylene) (MOPV) self-organize in chiral stacks in apolar solvents below a sharp transition temperature [13]. The secondary interactions used for the supramolecular assembly are quadrupolar hydrogen bonding, $\pi-\pi$ stacking and solvophobic effects. In this paper, we investigate supramolecular nanostructures consisting of a blend of MOPV3 and MOPV4 [14] (see Fig. 1 for the molecular structures and a schematic of the architecture). We have demonstrated previously that at low MOPV4 mole fraction ($\lesssim 2\%$), isolated MOPV4 chromophores are incorporated into MOPV3 helical assemblies as long as the solution is thermally cycled to dissolve and then re-assemble the stacks [15]. Optical excitation of the blended structure results in efficient energy transfer from MOPV3 hosts to MOPV4 guests, with most of the transfer occurring over the first 100 ps. Here, we investigate further the energy transfer process by applying time-resolved photoluminescence spectroscopy.

Resonance energy transfer (RET) is fundamental to describe exciton dynamics in conjugated structures. It has been shown that intermolecular energy transfer is the dominant mechanism in polymer films while intramolecular energy transfer determines exciton dynamics in dilute polymer solutions [16,17]. A quantitative study of intermolecular energy transfer in polymer films is complicated by the intrinsic positional and energy disorder of such systems. MOPV, on the other hand, is a model system to study energy transfer dynamics as it is possible to investigate the effect of intermolecular interactions by comparing optical properties of MOPV in the dissolved phase and the supramolecular assemblies. In supramolecular assemblies, the conjugated segments are closely packed in a fashion similar to conjugated segments in polymeric films but in a well-defined manner. In a previous paper, we have investigated exciton dynamics in MOPV4 with time-resolved photoluminescence spectroscopy and we found them to be very similar to those of polymeric films [18]. Fast exciton diffusion on chiral supramolecular assemblies was shown to lead to exciton trapping and luminescence depolarisation. We have also demonstrated, using femtosecond transient absorption spectroscopy, that exciton bimolecular annihilation dynamics in MOPV4 assemblies are dominated by a combination of exciton diffusion (over nearest-neighbour lengthscales and beyond), and long-range resonance energy interactions [19]. In the blend studies presented in this paper, we observe fast diffusion-assisted RET to MOPV4 and trapping in MOPV3 (over picosecond timescales), and direct RET dynamics from *localised* MOPV3 fluorophores to MOPV4 chromophores (over nanosecond timescales). Analysis of the photoluminescence kinetics on nanosecond timescales with a Förster model demonstrates significant RET interactions over long distances (~ 8 nm), with a quasi-one-dimensional donor–acceptor distribution.

2. Experimental

The synthesis and characterisation of MOPV3 and MOPV4 (see Fig. 1 for the molecular structures) has been described elsewhere [13,14]. The materials were dissolved in anhydrous dodecane. The MOPV3 concentration was kept around 1.4×10^{-4} M while the mole fractions of MOPV4 were varied by titration of MOPV4 dissolved in anhydrous dodecane. The MOPV4 mole fraction was varied from 0% to 13%. MOPV4 was incorporated into MOPV3 stacks by heating the solution to 80 °C after each titration to dissolve the stack, and then cooling the solution to a temperature well below the transition temperature for supramolecular assembly [14], usually 14–19 °C. Measurements were carried in a temperature-controlled, anaerobic fluorescence cuvette with 2 mm path length.
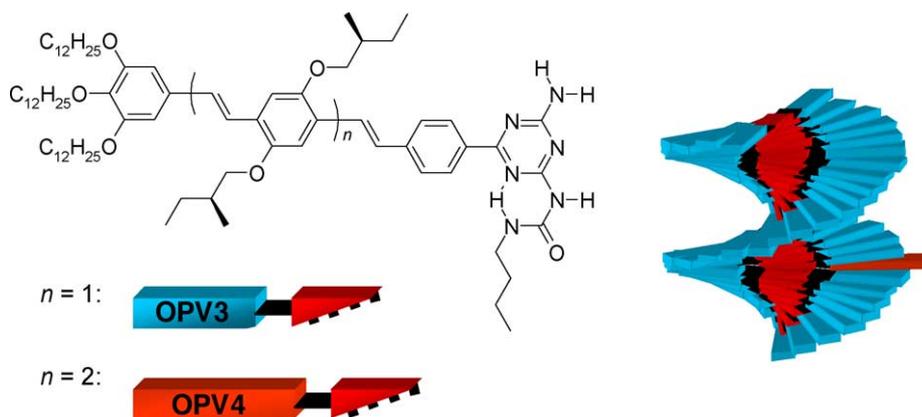

Fig. 1. Molecular structure of MOPV and schematic of the mixed columnar stacks of MOPV dimers in dodecane solution. The formation of mixed stacks is enabled by the hydrogen-bonding motif that end-caps both molecules.

Time-resolved photoluminescence measurements were carried out with two different techniques. To investigate picosecond dynamics, photoluminescence up-conversion (PLUC) spectroscopy was applied as described elsewhere [18]. Briefly, samples were photoexcited with the second harmonic (3.1 eV) of a Ti:sapphire oscillator (Coherent Mira) operating at 76 MHz. The laser fluence used for these experiments was 30 nJ cm^{-2}. The fluorescence emitted from the sample was up-converted in a β-BBO crystal using the residual fundamental pulses as a gate. Sum-frequency photons were directed into a monochromator and detected via single photon counting. The spectra were corrected for the response of the apparatus measured using a tungsten lamp of known emissivity. The instrument response in this experiment was 300 fs FWHM. Over timescales up to 50 ns, photoluminescence measurements were made by time-correlated single photon counting (TCSPC) as described in detail elsewhere [20]. The samples were excited with a pulsed 3.047 eV, 20 MHz, 70 ps FWHM diode laser (PicoQuant LDH 400) and their luminescence detected with a Peltier-cooled microchannel plate photomultiplier (Hamamatsu) coupled to a monochromator and TCSPC electronics (Lifespec-ps and VTC900 PC card, Edinburgh Instruments). The instrument response in this experiment was 100 ps FWHM.

3. Results and analysis

The materials investigated here are oligo-*p*-phenynevinylene derivatives consisting of three or four phenyl rings (MOPV3 and MOPV4, respectively), monofunctionalized with ureido-*s*-triazine. The latter group leads to dimer formation in dodecane solution by hydrogen bonding [12], and the resulting supramolecular structures are shown in Fig. 1. The photoluminescence (PL) spectrum of MOPV3 is peaked near 2.4 eV, and is overlapped significantly with the molar absorptivity spectrum of MOPV4 (Fig. 2). RET with significant efficiency is therefore expected. Fig. 3 displays the time-integrated PL spectrum of MOPV3 (part (a)), MOPV4
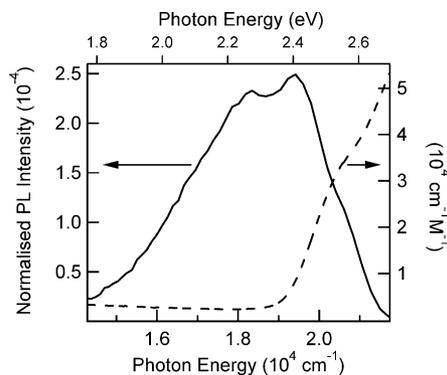
Fig. 2. Spectra of photoluminescence intensity ($f(\bar{v})$) of MOPV3 (left axis) and decadic molar absorptivity ($\varepsilon(\bar{v})$) of MOPV4 (right axis) supramolecular assemblies in ∼1 × 10^{-5} M dodecane solution. The photoluminescence spectrum is normalised such that $\int_0^\infty f(\bar{v}) \, d\bar{v} = 1$.
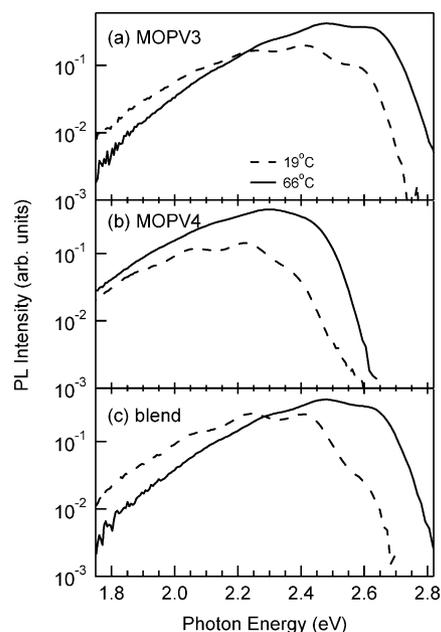
Fig. 3. Time-integrated photoluminescence spectra of (a) MOPV3 and (b) MOPV4 dodecane solutions (∼1 × 10^{-5} M), and (c) similar solution of a blend of MOPV4 (2.6% mole fraction) in MOPV3. The spectra were recorded at a solution temperature of 66 °C (continuous lines) and 19 °C (broken lines).

(part (b)), and a blend of the two oligomers with 2.6% mole fraction of MOPV4 (part (c)). At 66 °C, where the equilibrium is shifted away from supramolecular organisation [14], the PL spectrum of the blend is simply that of MOPV3 since the average donor–acceptor separation is too large for RET and direct excitation of the acceptor is unimportant at this low mole fraction. At 19 °C, where there is a high degree of supramolecular assembly, the spectrum of the blend is significantly red-shifted. We ascribe this shift to enhancement of the RET rate through π−π stacking. Furthermore, the integrated PL intensity decreases in the assembled versus dissolved system. We have previously demonstrated that in pure MOPV4, rapid diffusion-assisted exciton quenching occurs in the assembly [18]. This process is also likely to occur in MOPV3, and the time-integrated PL characteristics of the blend are determined by (i) competition of quenching of excitons in MOPV3, (ii) trapping and radiative decay in MOPV3, and (iii) radiative decay in MOPV4 resulting from RET.

In order to explore the RET process, we have undertaken PLUC measurements on the blend solution discussed above, with results displayed in Fig. 4. The solution at 19 °C displays a significant dynamic red shift during the first 600 ps. Between 300 fs and 600 ps after photoexcitation, the average PL photon energy, defined by $\left[\int_0^\infty f(E)E \, dE \right] / \left[\int_0^\infty f(E) \, dE \right]$ with $f(E)$ being the PL intensity with photon energy E, decreases by 114 meV, with 59% of that relaxation occurring over the first 25 ps. This is much larger than the ∼ 30 meV dynamic shift in MOPV4 [18]. However, the spectrum does not undergo a simple dynamic red shift; the decay of the
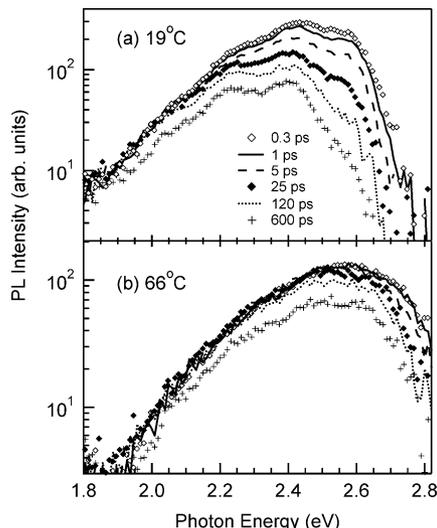
Fig. 4. Time-resolved photoluminescence spectra of a blend of MOPV3 and MOPV4 (2.6% by volume) in dodecane. The data were recorded at (a) 19 °C and (b) 66 °C.
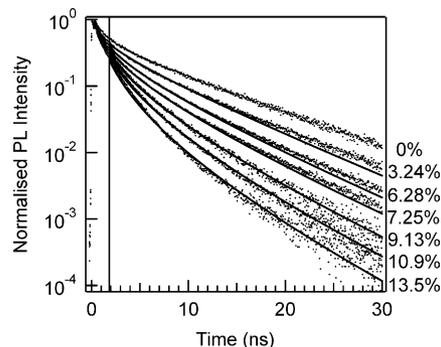

Fig. 5. Photoluminescence decay at 2.610 eV photon energy of MOPV3 and blends of MOPV4 in MOPV3 at 14 °C. The MOPV3 concentration was kept around 1.4×10^{-4} M while the mole fractions of MOPV4 were varied as indicated in the figure. The lines through the data result from a global fit to $I(t)$ (Eq. (4)) in the time window spanning 1.86–30 ns (indicated by the vertical line), with $k = 0.126 \, \text{ns}^{-1}$ and $c = 0.212$.

region around 2.6 eV is much more rapid than that at 2.2 eV, leading to a dynamic narrowing of the spectrum. This arises from the concomitant decrease in MOPV3 population (which emits predominantly in the blue edge of the spectral range in Fig. 4) and rise in MOPV4 population resulting from RET.

We now turn to RET dynamics on nanosecond timescales, which involves transfer from localised [18] fluorophores. In MOPV stacks, RET involving nearest-neighbour interactions are not adequately described with Förster theory due to the breakdown of the point-dipole approximation [17] resulting from the non-negligible size and shape of the excited-state wavefunctions compared to the donor–acceptor separation. However, at sufficiently low acceptor mole fraction and at low exciton densities on MOPV3, and if homotransfer (i.e. exciton diffusion) dynamics in MOPV3 are negligible, then RET processes can be described with a Förster model since on average the donor–acceptor separation on nanosecond timescales is such that the point-dipole approximation is reasonable. With this approximation, a one-step Förster model predicts a time dependence of the excitation transfer rate of $t^{(\Delta/6)-1}$, with Δ being the dimensionality of the acceptor distribution. This result is the generalisation of the methodology developed by Eisenthal and Siegel [21] for three-dimensional RET to a situation with arbitrary dimensionality. The time-dependent population of the donor exciton density, n, after pulsed photoexcitation is governed by the following rate equation:

$$\frac{\text{d}}{\text{d}t} n(t) = g(t) - \frac{n(t)}{\tau} - \gamma t^{(\Delta/6-1)} n(t) \tag{1}$$

Here $g(t)$ is the exciton generation function, τ the excited-state lifetime of the donor in the absence of acceptors, and γ is the rate constant for RET. If the excitation pulse is very short compared to the characteristic timescales of τ and γ, we may approximate $g(t) = n_0 \, \delta(t)$, where n_0 is the $t = 0$ exciton

density of the donor. The time-dependent donor population density is then given by

$$n(t) = n_0 \exp\left(-\frac{t}{\tau} - \frac{6\gamma}{\Delta} t^{\Delta/6}\right) \tag{2}$$

with γ given by

$$\gamma = \Re^\Delta \rho_\Delta \frac{\Delta \pi^{\Delta/2} \Gamma(1 - \Delta/6)}{6\Gamma(1 + \Delta/2)\tau^{\Delta/6}} \tag{3}$$

where Γ is the gamma function, $\Re$ the Förster radius and ρ_Δ is the acceptor density in Δ dimensions with units $m^{-\Delta}$.

We have measured time-dependent PL intensity at 2.61 eV photon energy with TCSPC in order to explore RET processes on nanosecond time scales. Fig. 5 displays the PL decay kinetics of various MOPV4/MOPV3 blend solutions with mole fraction of MOPV4 ranging from 0% (pure MOPV3) to 13.5%. This emission photon energy primarily probes population in MOPV3. Pure MOPV3 displays non-exponential decay kinetics over timescales up to ~2 ns, but at longer timescales the decay is exponential with a time constant of $\tau = (7.94 \pm 0.02)$ ns. We have reported previously that the decay of PL displays stretched exponential behaviour on sub-nanosecond timescales arising from diffusion-assisted exciton quenching on MOPV stacks [18]. We therefore consider only decay kinetics after ~2 ns in the following analysis.

In order to extract $\Re$ and Δ from the data in Fig. 5, we have applied a global fit to PL decays at 16 different MOPV4 mole fractions with

$$I(t) = \alpha \exp(-kt - bt^{-c}) \tag{4}$$

where k was fixed to $\tau^{-1} = 0.126 \, \text{ns}^{-1}$ obtained from an exponential tail fit of the 0% acceptor mole fraction data, a and b were allowed to float for each individual data set, and c was only allowed to float globally for the entire data set. The best global fits (shown in Fig. 5 for the displayed transients) yields $c = 0.212 \pm 0.010$. Comparison of Eqs. (2) and (4) leads to $\Delta = 1.3 \pm 0.1$. We find that if we constrain the value of c to 0.5, corresponding to a three-dimensional acceptor distribution,
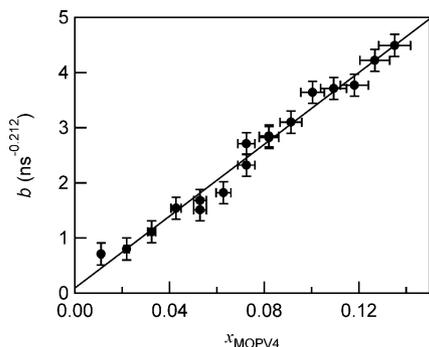
Fig. 6. Parameter *b* (Eq. (4)) as a function of mole fraction of MOPV4 in blends of MOPV3 and MOPV4 in dodecane solution at 14 °C, obtained from a global fit of the decay of photoluminescence intensity (Fig. 5 at various mole fractions of MOPV4.

the goodness-of-fit deduced by statistical analysis of the χ^2 values is at least a factor of two worse than if *c* is allowed to float freely. In the mixed MOPV structure, $\rho_{\Delta=1}$ is defined by the stack and is given by $x/\bar{\tau}$, where *x* is the MOPV4 mole fraction and $\bar{\tau} = 0.35$ nm [22] is the average intermolecular separation. Therefore, from the slope of a plot of *b* versus *x*, shown in Fig. 6, and from Eq. (3), we determine a Förster radius of $\Re = (7.8 \pm 1.7)$ nm. This analysis suggests a one-dimensional distribution of MOPV4 acceptors in a MOPV3 donor stack, with significant donor–acceptor electronic coupling over long ranges.

4. Discussion

We have established that RET from MOPV3 hosts to MOPV4 guests in mixed supramolecular stacks of the two oligomers is efficient. The picture emerging from Section 3 is the following. At low MOPV4 mole fraction, a significant extent of RET occurs within the first ∼100 ps after absorption of light by MOPV3. During this time, significant exciton diffusion occurs in MOPV3 [18], which assists exciton transfer to MOPV4.

A quantitative description of the processes in this fast (sub-nanosecond) time-scale is beyond the scope of this paper. Firstly, it would require a statistical treatment of microscopic events within the mixed MOPV stack. Secondly, an appropriate description of the donor–acceptor electronic coupling is more complex than that afforded by Förster theory. Meskers et al. [23] have discussed the photoexcitation relaxation dynamics in aggregates of OPVs in situations where the degree of energetic disorder is low. In this situation, excitonic states that are delocalised between several molecules predominate, and the luminescence is induced by vibronic mixing of the molecular excited states. This leads to an emission bandshape that is different from that of the isolated oligomers, as we indeed observe in Fig. 3. (The changes in the PL characteristics depend on the strength of the intermolecular electronic coupling with respect to the intramolecular relaxation energy and on disorder.) A full representation of the RET dynamics in

this situation requires a model that goes beyond Förster theory in the description of the intermolecular electronic coupling [17] and, depending on the magnitude of this coupling, perhaps away from the golden rule rate expression derived from second-order perturbation theory [24].

Exciton trapping occurs within a ∼1 ns timecale in MOPV stacks [18]. In contrast to the situation described above, RET processes in this regime can be described adequately with Förster theory as long as three conditions are met. The first is that multi-step homotransfer dynamics in MOPV3 are negligible. The second is that the exciton density in MOPV3 is sufficiently low so that exciton bimolecular processes [19] are not important. The third is that the MOPV4 (acceptor) mole fraction is sufficiently low so that on average the donor–acceptor separation is much longer than the nearest-neighbour separation to avoid the complications imposed by the break-down of the point-dipole approximation [17]. We consider that the data in Fig. 5 meet these conditions. Our analysis of the time-resolved PL data on nanosecond timescales with a dimensionally-generalised Förster model is consistent with a one-dimensional acceptor distribution. We note that the Förster radius of 8 nm extracted from this model is consistent with the optimum MOPV4/MOPV3 composition of 1.9 mol% MOPV4 found by steady-state PL measurements and using a Stern–Volmer analysis [15].

We can compare the Förster radius, which defines the characteristic length at which the rate of RET is equal to all other excited-state deactivation processes, with that determined directly from the spectral overlap shown in Fig. 2. Förster expressed this as [25]

$$\Re = \left[\frac{9000 \ln 10 \kappa^2 \eta}{128 \pi^5 n^4 N_A} \int_0^\infty f_D(\bar{\nu}) \varepsilon_A(\bar{\nu}) \frac{d\bar{\nu}}{\bar{\nu}^4} \right]^{1/6} \quad (5)$$

where κ^2 is the orientation factor of the donor and acceptor dipole moments, η the PL efficiency of the donor, *n* the refractive index of the medium, N_A Avogadro's number, f_D is the fluorescence spectrum of the donor with integrated intensity normalised to unity in a wavenumber energy scale, and ε_A is the molar absorptivity spectrum of the acceptor. This expression of $\Re$ is independent of dimensionality of the acceptor distribution, since it only relates to the spatial distribution of the dipole radiation field. Using Eq. (5) with $\langle \kappa^2 \rangle = 0.45$ (determined by averaging over all possible donor–acceptor orientations in the stack), we compute a characteristic radius $\Re = 3.9$ nm. This is roughly a factor of two smaller than the value of $\Re$ determined from the global fit to the time-resolved PL data. We point out, however, that Eq. (5) is strictly valid only for homogeneously broadened spectra, which is not the case in these MOPV stacks. It is also incorrect to use the absorption spectrum of pure MOPV4 assemblies in Eq. (5) because the acceptor is embedded in MOPV3 structures, although we expect that this approximation is of minor consequence. Finally, the Förster formalism is not valid in the strong exciton coupling limit [26]. As this system is in the intermediate regime, discrepancies can be expected but a proper

description would need to take into account the exciton relaxation that occurs on ultrafast timescales.

In a previous publication describing femtosecond-resolved transient PL measurements in MOPV4 [18], we found that a stretched exponential function of the form $I(t) = I_0 \exp(-t/\tau)^\beta$ describes the PL decay of the supramolecular assemblies. At the lowest solution temperature that was measured (19 °C), $\beta = 1/3$ over the first 600 ps. We invoked models relating β to the lattice dimensionality d by $\beta = d/(d + 2)$. Note that d and Δ discussed here have slightly different meaning; the dimensionality of the lattice in which excitons undergo multiple incoherent hops during their lifetime is d, whereas here Δ is the dimensionality of the donor–acceptor distribution in one-step transfer processes. Although these models do not explicitly take into account energetic disorder, we argued that multistep exciton diffusion in a quasi-one-dimensional lattice is a plausible description of exciton dynamics in MOPV over this short timescale because nearest-neighbour interactions are expected to play a dominant role. At longer times (>2 ns) we invoked a higher dimensionality of the donor–acceptor distribution, as excitons located in a local minimum of the potential energy landscape need to interact with suitable transfer sites that are located further away and the probability of transfer to sites in the opposite helix of the architecture is non-negligible. This is a picture that is also consistent with MOPV3 stacks; the pure MOPV3 data in Fig. 5 display non-exponential decay at early time, switching to exponential decay after a few nanoseconds as reported in the case of MOPV4 [18].

The situation changes upon addition of deeper traps in the form of MOPV4 to MOPV3 stacks, where PL decay on nanosecond timescales becomes non-exponential again and the distribution of suitable acceptor sites displays quasi-one-dimensional characteristics once again. In light of the observation that at MOPV4 incorporation ratios higher than ~2% mole fraction the guest molecules appear to interact and are not incorporated as isolated traps [15], it is plausible that localised excitons in MOPV3 undergo *single* step transfer and see a predominantly one-dimensional distribution of MOPV4.

This scenario appears to be distinct from that invoked to describe exciton bimolecular annihilation processes in MOPV4 [19]. In that case, a bimolecular annihilation rate constant with explicit time dependence in the form $t^{-1/2}$ was required to reproduce femtosecond transient absorption data at high pump fluences ($\geq 100 \,\mu J \, cm^{-2}$). We interpreted this as indicative of a non-Markovian exciton bimolecular depletion mechanism mediated by long-range RET interactions. In contrast to the analysis presented here, an effective three-dimensional exciton distribution was deduced from the exponent of the time dependence of the bimolecular annihilation rate constant. We reconcile this with the analysis presented here by pointing out that the bimolecular annihilation process occurs in a picosecond timescale where the exciton diffusivity is high and sites close to acceptor sites in the opposite helix can be reached more readily by multiple hops, rendering the apparent acceptor distribution to have a higher dimensionality than one. We pointed out that for this reason, a microscopic description is more adequate to describe the bimolecular annihilation phenomena.

5. Conclusions

We have applied time-resolved photoluminescence spectroscopy to investigate the resonance energy transfer dynamics in mixed supramolecular stacks of two oligo-*p*-phenylenevinylene derivatives with different conjugation lengths. Efficient RET is observed on sub-nanosecond timescales, indicated by rapid depletion of donor PL intensity and concomitant rise of acceptor PL intensity. In this time regime, highly mobile excitons in the donor migrate to sites near acceptors. At longer timescales, when exciton localise in a local potential energy minimum, excitons transfer to acceptor sites over long distances. A simple Förster model adequately describes these dynamics, yielding a Förster radius of 8 nm, with a quasi-one-dimensional donor–acceptor distribution. Control of order in the nanometre lengthscale provides a promising strategy for harvesting energy in supramolecular semiconductor systems.

References

[1] N. Stutzmann, R.H. Friend, H. Sirringhaus, Science 299 (2003) 1881.
[2] R.H. Friend, R.W. Gymer, A.B. Holmes, J.H. Burroughes, R.N. Marks, C. Taliani, D.D.C. Bradley, D.A. DosSantos, J.L. Brédas, M. Lögdlund, W.R. Salaneck, Nature 397 (1999) 121.
[3] C.J. Brabec, C. Winder, N.S. Sariciftci, J.C. Hummelen, A. Dhanabalan, P.A. van Hal, R.A.J. Janssen, Adv. Funct. Mater. 12 (2002) 709.
[4] S. Setayesh, A.C. Grimsdale, T. Weil, V. Enkelmann, K. Müllen, F. Meghdadi, E.J.W. List, G. Leising, J. Am. Chem. Soc. 123 (2001) 946.

[5] A.C. Grimsdale, P. Leclere, J.D. Mackenzie, C. Murphy, S. Setayesh, C. Silva, R.H. Friend, K. Müllen, Adv. Funct. Mater. 12 (2002) 729.

[6] C. Ego, D. Marsitzky, S. Becker, J.Y. Zhang, A.C. Grimsdale, K. Müllen, J.D. Mackenzie, C. Silva, R.H. Friend, J. Am. Chem. Soc. 125 (2003) 437.

[7] H. Sirringhaus, P.J. Brown, R.H. Friend, M.M. Nielsen, K. Bechgaard, B.M.W. LangeveldVoss, A.J.H. Spiering, R.A.J. Janssen, E.W. Meijer, P. Herwig, D.M. de Leeuw, Nature 401 (1999) 685.

[8] H. Sirringhaus, T. Kawase, R.H. Friend, T. Shimoda, M. Inbasekaran, W. Wu, E.P. Woo, Science 290 (2000) 2123.

[9] T. Kawase, H. Sirringhaus, R.H. Friend, T. Shimoda, Adv. Mater. 13 (2001) 1601.

[10] J.M. Lehn, Supramolecular Chemistry, VCH, Weinheim, 1995.

[11] A.M. van de Craats, J.M. Warman, A. Fechtenkötter, J.D. Brand, M.A. Harbison, K. Müllen, Adv. Mater. 11 (1999) 1469.

[12] A.P.H.J. Schenning, P. Jonkheijm, F.J.M. Hoeben, J.V. Herrikhuyzen, S.C.J. Meskers, E.W. Meijer, L.M. Herz, C. Daniel, C. Silva, R.T. Phillips, R.H. Friend, D. Beljonne, A. Miura, S. De Feyter, M. Zdanowska, H. Uji-i, F.C. De Schryver, Z. Chen, F. Wiirthner, M. Mas-Torrent, D. den Boer, M. Durkut, P. Hadley, Synth. Met. (this issue).

[13] A.P.H.J. Schenning, P. Jonkheim, E. Peeter, E.W. Meijer, J. Am. Chem. Soc. 123 (2001) 409.

[14] P. Jonkheijm, F.J.M. Hoeben, R. Kleppinger, J. van Herrikhuyzen, A.P.H.J. Schenning, E.W. Meijer, J. Am. Chem. Soc. 125 (2003) 15941.

[15] F.J.M. Hoeben, L.M. Herz, C. Daniel, P. Jonkheijm, A.P.H.J. Schenning, C. Silva, S.C.J. Meskers, D. Beljonne, R.T. Phillips, R.H. Friend, E.W. Meijer, Angew. Chem. 43 (2004) 1976.

[16] T.-Q. Nguyen, J. Wu, V. Doan, B.J. Schwartz, S.H. Tolbert, Science 288 (2000) 652.

[17] D. Beljonne, G. Pourtois, C. Silva, E. Hennebicq, L.M. Herz, R.H. Friend, G.D. Scholes, S. Setayesh, S. Becker, D. Marsitsky, K. Müllen, J.L. Brédas, Proc. Nat. Acad. Sci. U.S.A. 99 (2002) 10982.

[18] L.M. Herz, C. Daniel, C. Silva, F.J.M. Hoeben, A.P.H. Schenning, E.W. Meijer, R.H. Friend, R.T. Phillips, Phys. Rev. B 68 (2003) 045203.

[19] C. Daniel, L.M. Herz, C. Silva, F.J.M. Hoeben, A.P.H.J. Schenning, E.W. Meijer, Phys. Rev. B 68 (2003) 235212.

[20] A.C. Morteani, A.S. Dhoot, J.-S. Kim, C. Silva, N.C. Greenham, R.H. Friend, C. Murphy, E. Moons, S. Ciná, J. Burroughes, Adv. Mat. 15 (2003) 1708.

[21] K.B. Eisenthal, S. Siegel, J. Chem. Phys. 41 (1964) 652.

[22] The intermolecular separation was determined by molecular mechanics calculations based on the Dreiding force field.

[23] S.C.J. Meskers, R.A.J. Janssen, J.E.M. Haverkort, J.H. Wolter, Chem. Phys. 260 (2000) 415.

[24] V. May, O. Kühn, Charge and Energy Transfer Dynamics in Molecular Systems, Wiley, Berlin, 2000.

[25] T. Förster, Disc. Faraday Soc. 27 (1959) 7.

[26] G.D. Scholes, Annu. Rev. Phys. Chem. 54 (2003) 57.